JACS
JOURNAL OF THE AMERICAN CHEMICAL SOCIETY
Article
pubs.acs.org/JACS

Mechanism of Asymmetric Hydrogenation of Aromatic Ketones Catalyzed by a Combined System of Ru(π-$CH_2C(CH_3)CH_2)_2$(cod) and the Chiral sp^2N/sp^3NH Hybrid Linear N4 Ligand Ph-BINAN-H-Py

Hiroshi Nakatsuka,[†] Tomoya Yamamura,[†] Yoshihiro Shuto,[†] Shinji Tanaka,[†] Masahiro Yoshimura,[‡] and Masato Kitamura*,[†]

[†]Graduate School of Pharmaceutical Sciences, Graduate School of Science, and Research Center for Materials Science, Nagoya University, Chikusa, Nagoya 464-8601, Japan

[‡]Division of Liberal Arts and Sciences, Aichi Gakuin University, Iwasaki, Nisshin 470-0195, Japan

Supporting Information

ABSTRACT: The combination of a Goodwin–Lions-type chiral N4 ligand, (*R*)-Ph-BINAN-H-Py ((*R*)-3,3′-diphenyl-N^2,$N^{2\prime}$-bis((pyridin-2-yl)methyl)-1,1′-binaphthyl-2,2′-diamine; **L**), with Ru(π-$CH_2C(CH_3)CH_2)_2$(cod) (**A**) (cod = 1,5-cyclooctadiene) catalyzes the hydrogenation of acetophenone (**AP**) to (*R*)-1-phenylethanol (**PE**) with a high enantiomer ratio (er). Almost no Ru complex forms, with **A** and **L** remaining intact throughout the reaction while generating **PE** quantitatively according to [**PE**] = $k_{obs}t^2$. An infinitesimal amount of reactive and unstable RuH_2**L** (**B**) with C_2-Λ-*cis*-α stereochemistry is very slowly and irreversibly generated from **A** by the action of H_2 and **L**, which rapidly catalyzes the hydrogenation of **AP** via Noyori's donor–acceptor bifunctional mechanism. A CH-π-stabilized *Si*-face selective transition state, $\mathbf{C}_{Si}$, gives (*R*)-**PE** together with an intermediary Ru amide, **D**, which is inhibited predominantly by formation of the Ru enolate of **AP**. The rate-determining hydrogenolysis of **D** completes the cycle. The time-squared term relates both to the preliminary step before the cycle and to the cycle itself, with a highly unusual eight-order difference in the generation and turnover frequency of **B**. This mechanism is fully supported by a series of experiments including a detailed kinetic study, rate law analysis, simulation of t/[**PE**] curves with fitting to the experimental observations at the initial reaction stage, X-ray crystallographic analyses of **B**-related octahedral metal complexes, and Hammett plot analyses of electronically different substrates and ligands in their enantioselectivities.

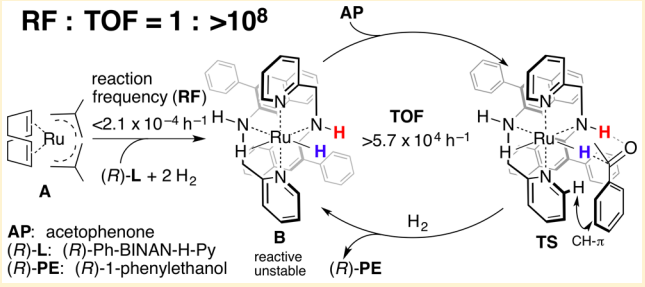

1. INTRODUCTION

Since the BINAP–Ru method made its debut in 1987,[1] homogeneous asymmetric hydrogenation of ketones has become established as one of the most reliable strategies for the synthesis of optically active secondary alcohols. The first report on homogeneous ketone hydrogenation dates back as far as 1938, when Calvin demonstrated the catalytic activity of $CuOCOCH_3$.[2] In the shadow of immense efforts toward the development of homogeneous catalysts for olefin hydrogenation using Rh, Ru, or Pt complexes in combination with various organic ligands,[3] little progress in this area was made until 1970, when Schrock and Osborn discovered the high utility of monocationic $RhH_2(PPhMe_2)_2(solvent)_2$ in the hydrogenation of acetone to 2-propanol.[4] Their discovery triggered an increase in the number of studies using chiral phosphines,[5] eventually leading to the revolutionary catalyst system consisting of $Ru(OCOCH_3)_2$(BINAP) and a strong Brønsted acid.[1] The first generation of BINAP–Ru chemistry realized the hydrogenation of β-keto esters and a wide range of functionalized ketones with nearly perfect enantioselectivity,[6] the successful development of which relies on the concept of an intermolecular-type donor–acceptor bifunctional catalyst (Intermol-DACat) (Figure 1a).[1c,7]

A second revolution took place in 1995, when a chiral Ru catalyst consisting of $RuCl_2$(BINAP)$(dmf)_n$[8] and 1,2-diphenylethane-1,2-diamine (DPEN) was developed.[9] This BINAP–Ru–DPEN ternary system, which was based on the concept of an intramolecular-type donor–acceptor bifunctional catalyst (Intramol-DACat) (Figure 1b), shows high efficiency in the hydrogenation of unfunctionalized ketones. Since the start of this apparent trend of BINAP–Ru systems, a vast number of hydrogenation-active Ru complexes with trivalent phosphorus ligating atoms have been reported.[10] Their effectiveness has been examined and compared to that of the "privileged"[11] BINAP chiral catalyst and its derivatives. Nevertheless, no omnipotent catalyst exists even now, and new frameworks for designing asymmetric catalysts are required.

From this viewpoint, nitrogen-based ligands have hidden potential because they have not been extensively researched as

Received: March 5, 2015
Published: June 5, 2015

DOI: 10.1021/jacs.5b02350
J. Am. Chem. Soc. 2015, 137, 8138–8149

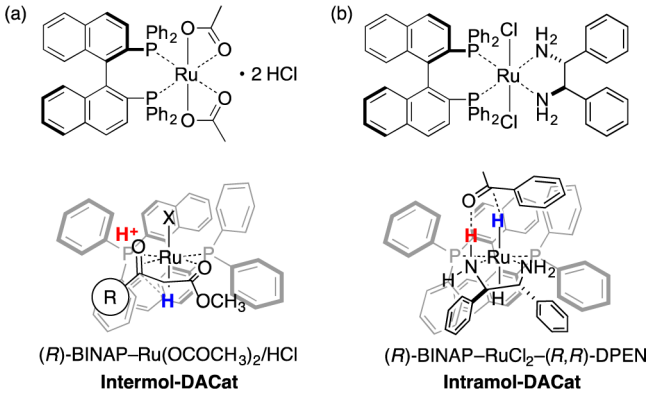

Figure 1. Two epoch-making asymmetric hydrogenation reactions of ketones and the underlying concepts.

yet, although Ohgo et al. reported the first asymmetric hydrogenation of ketones catalyzed by Co(II)-(bisdimethylglyoximato)/quinine in 1971,[12] around the same time as Schlock–Osborn's report.[4] After three unproductive decades, there is now increasing attention on all nitrogen-ligating systems. The Goodwin–Lions-type tetradentate sp^2N/sp^3NH linear N4 ligand *R*-BINAN-*R*′-Py (3,3′-*R*,*R*-N^2,$N^{2'}$-bis((6-*R*′-pyridin-2-yl)methyl)-1,1′-binaphthyl-2,2′-diamine)[13,14] is one of the key examples setting a precedent in this new trend.[15] A combination of the nonphosphine ligand Ph-BINAN-H-Py (**L**) and the Ru π-allyl complex Ru(π-$CH_2C(CH_3)CH_2)_2$(cod) (**A**)[16] quantitatively hydrogenates various aromatic ketones with a substrate/catalyst (S/C) ratio of >10 000 to give the secondary alcohol with an enantiomer ratio (er) of up to >99:1.[13] *Most interestingly, the reaction proceeds with almost no formation of any Ru complexes.* Here, we would like to present a mechanism explaining this unusual phenomenon and the origin of enantioselection in the (*R*)-**L**/**A**-catalyzed asymmetric hydrogenation of acetophenone (**AP**) to (*R*)-1-phenylethanol ((*R*)-**PE**) (Figure 2).

2. RESULTS AND DISCUSSION

2.1. Characteristic Features of (*R*)-Ph-BINAN-H-Py ((*R*)-L). *2.1.1. Λ-cis-α Selectivity.* Theoretically, the linear

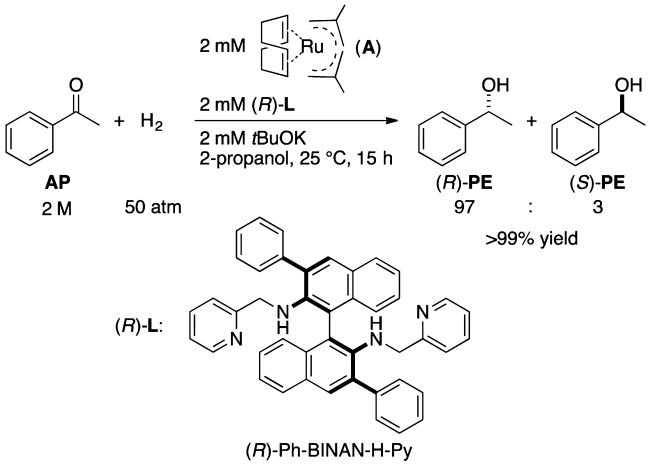

Figure 2. Standard conditions used for this mechanistic study of asymmetric hydrogenation of acetophenone (**AP**) catalyzed by the (*R*)-Ph-BINAN-H-Py/Ru(π-$CH_2C(CH_3)CH_2)_2$(cod) ((*R*)-**L**/**A**) combined system (**PE** = 1-phenylethanol).

tetradentate chiral ligand (*R*)-**L** can form five geometrical isomers in an octahedral metal complex[13]—C_2-Λ-*cis*-α-, C_2-Δ-*cis*-α-, C_1-Δ-*cis*-β-, C_1-Λ-*cis*-β-, and C_2-*trans*-isomers—although the C_2 symmetric Δ-*cis*-α and C_1 symmetric Λ-*cis*-β isomers are unlikely because of their highly distorted structures. These isomers are in equilibrium with each other (Figure 3a), and the

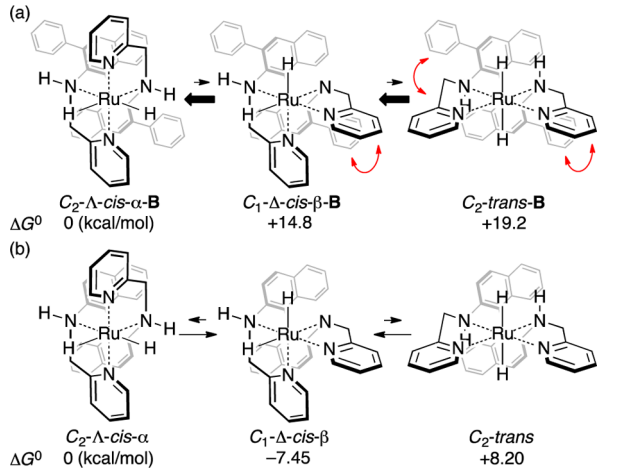

Figure 3. Equilibrium between three stereoisomers of (*R*)-Ph-BINAN-H-Py–RuH_2 (**B**) (a) and (*R*)-H-BINAN-H-Py–RuH_2 (b). Red arrows indicate a steric repulsion.

overall catalyst performance is the average of each isomer's own reactivity and enantioselectivity.[17] A density functional theory (DFT) calculation of an imaginary RuH_2((*R*)-**L**) (**B**) complex using the B3LYP/LANL2DZ set showed that the relative Gibbs free energies of Δ-*cis*-β-**B** and *trans*-**B** isomers are, respectively, 14.8 and 19.2 kcal/mol higher than that of Λ-*cis*-α-**B**. Steric repulsion (red arrow) between the C(3) phenyl group of the naphthalene ring and the pyridylmethyl group in the Δ-*cis*-β and *trans* isomers would shift the equilibrium to the Λ-*cis*-α-**B** side. The energy difference indicates that the Δ-*cis*-β-**B** and *trans*-**B** isomers exist at, respectively, only one-trillionth and one hundred-trillionth of the level of Λ-*cis*-α-**B**. This property is advantageous for unifying the catalytic species to enhance catalyst performance. Regarding the original Goodwin–Lions ligand,[14] which has no 3,3′-phenyl substituents of (*R*)-**L**, the C_1 symmetric Δ-*cis*-β isomer is the most stable (Figure 3b) according to the same DFT calculation. The existence of the two different possible reaction sites in the Δ-*cis*-β isomer may complicate the reaction pathways. In this sense, the C_2 symmetric Λ-*cis*-α-**B** isomer is simple.

2.1.2. Metal Capturing Ability. [Ru((*R*)-**L**)$(CH_3CN)_2$]-$(PF_6)_2$ (**1**) was quantitatively prepared by mixing (*R*)-**L** and $[Ru(C_6H_6)(CH_3CN)_3](PF_6)_2$[18] in CH_3CN at room temperature (rt) for 48 h, and yellowish prism crystals (melting point (mp) = 245 °C) were obtained in 68% yield from a $CHCl_3$–THF (THF = tetrahydrofuran) solvent system. Ru-$(OCOCH_3)_2$-((*R*)-**L**) (**2**) was also quantitatively obtained from $Ru_2(OCOCH_3)_4$[19] (CH_3OH, rt/48 h then 60 °C/2 h) and crystallized as reddish-brown platelets (mp = 225 °C) in 60% yield from CH_2Cl_2 and hexane. In a similar way, $Mn(OTf)_2$((*R*)-**L**) (60 °C, 30 min, CH_3CN), $Fe(OTf)_2$((*R*)-**L**) (25 °C, 1 h, THF), and $Cu(OTf)_2$((*R*)-**L**) (25 °C, 1 h, C_2H_5OH) were prepared.[20] The molecular structures in crystal are shown in Figure 4, reflecting a general tendency of (*R*)-Ph-BINAN-H-Py ligand ((*R*)-**L**) to form the C_2-Λ-*cis*-α isomer.

DOI: 10.1021/jacs.5b02350
J. Am. Chem. Soc. 2015, 137, 8138–8149

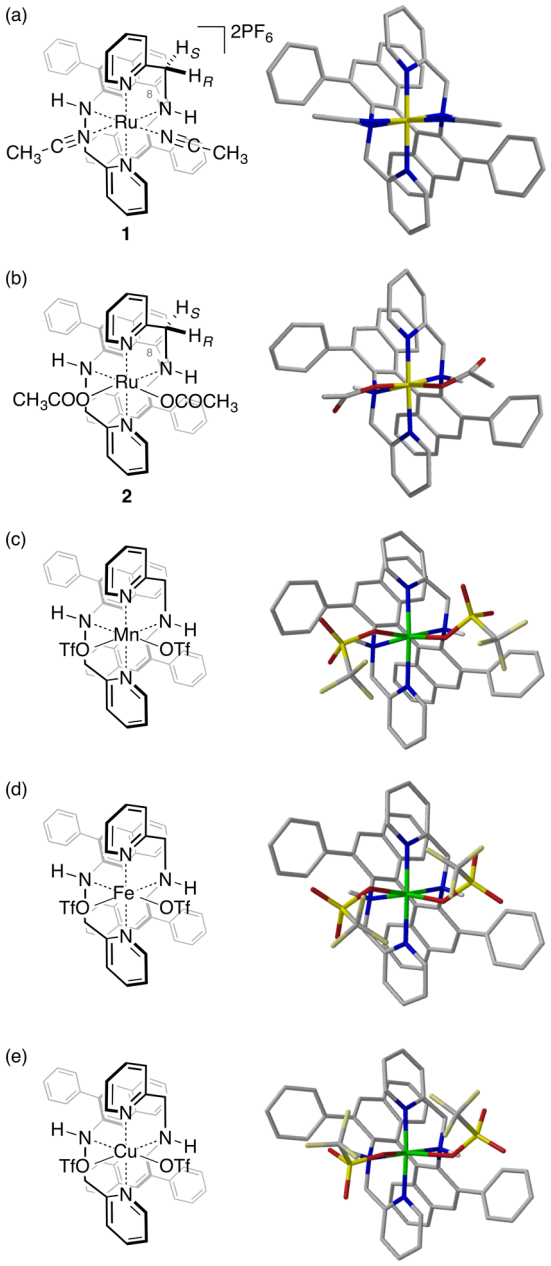

Figure 4. Molecular structures of (a) [Ru((*R*)-Ph-BINAN-H-Py)-$(CH_3CN)_2$]$(PF_6)_2$, (b) $Ru(OCOCH_3)_2$((*R*)-Ph-BINAN-H-Py), (c) $Mn(OTf)_2$((*R*)-Ph-BINAN-H-Py), (d) $Fe(OTf)_2$((*R*)-Ph-BINAN-H-Py), and (e) $Cu(OTf)_2$((*R*)-Ph-BINAN-H-Py) in the crystalline state. OTf = OSO_2CF_3.

The structure of Λ-*cis*-*α* in solution was confirmed by ^{1}H NMR analyses of two diamagnetic Ru complexes, [Ru((*R*)-**L**)$(CH_3CN)_2$]$(PF_6)_2$ (**1**) and $Ru(OCOCH_3)_2$((*R*)-**L**) (**2**). For both complexes, only one set of signals was observed in the ^{1}H NMR spectra:[20] (*R*)-**1** (*δ* 4.23 (dd, *J* = 18.6 and 5.5 Hz, CH_RH_S), 4.58 (dd, *J* = 18.6 and 8.9 Hz, CH_RH_S), 6.35 (dd, *J* = 8.9 and 5.5 Hz, NH)) and (*R*)-**2** (*δ* 1.46 (s, CH_3COO), 3.97 (dd, *J* = 17.2 and 6.0 Hz, CH_RH_S), 4.29 (dd, *J* = 17.2 and 8.1 Hz, CH_RH_S), 9.13 (dd, *J* = 8.1 and 6.0 Hz, NH)). These simple spectra were consistent with both complexes **1** and **2** having a symmetric C_2-Λ-*cis*-*α* structure. In addition, this Λ-*cis*-*α* geometry in solution phase was supported by the observation of a nuclear Overhauser effect (NOE) between the closely located naphthalene C(8)H and methylene H_S [(*R*)-**1**, 1.6% (irradiation of H_S) and 1.0% (irradiation of C(8)H); (*R*)-**2**, 3.5% (irradiation of H_S)].

2.2. Proposed Reactive Species: Λ-*cis*-*α*-RuH_2((*R*)-L) (B). *2.2.1. Catalyst Performance.* The above preformed Ru complexes (2 mM), Λ-*cis*-*α*-[Ru((*R*)-**L**)$(CH_3CN)_2$]$(PF_6)_2$ (**1**) and Λ-*cis*-*α*-$Ru(OCOCH_3)_2$((*R*)-**L**) (**2**), quantitatively hydrogenate acetophenone (**AP**) (2 M) in 2-propanol (*i*PrOH) containing potassium *tert*-butoxide (*t*BuOK) (20 mM) to give (*R*)-1-phenylethanol ((*R*)-**PE**) and (*S*)-**PE** with an er of, at most, 93:7 for complex **1** (H_2, 100 atm, 50 °C, 24 h) and 84:16 for complex **2** (H_2, 50 atm, 25 °C, 24 h).[20] In contrast to the present (*R*)-**L**/**A** combined system (Figure 2) and against expectation, the catalyst performance of that system was low. The RuX_2−**L**-type complexes require an excess amount of base, because the balance point lies toward the left side in the equilibria of both "RuX_2−**L** + H_2 ⇄ RuHX−**L** + HX" and "RuHX−**L** + H_2 ⇄ RuH_2−**L** + HX".[21a,22c] The reaction system might be complicated by the remaining *t*BuOK and coproduced salts such as KPF_6 and $KOCOCH_3$, which might disturb the clean generation of the presumed reactive species, Λ-*cis*-*α*-RuH_2((*R*)-**L**) (**B**).

2.2.2. Trial for Detection of B. Related mechanistic studies on the hydrogenation of ketones using Ru complexes of phosphine-containing ligands suggest that a RuH_2 mechanism operates.[21−24] Furthermore, RuH_2 complexes can be prepared in high yields from Ru(*π*-$CH_2C(CH_3)CH_2)_2$(diphosphine) and Ru(*π*-$CH_2C(CH_3)CH_2)_2$(cod) (**A**)/PNP ligand.[25] On the basis of this information, we tried to detect either RuH_2((*R*)-**L**) (**B**) or any Ru complexes from **A** and **L** with or without H_2 and at 25 or 60 °C, but in vain (Table 1).[20] Nothing occurred at 25 °C, but a black precipitate, most probably a Ru(0) cluster

Table 1. Results of the Trial for Detection of Ph-BINAN-H-Py−RuH_2 (B)[a]

				% convn[b]		% yield[b]	
entry	solvent	H_2, atm	temp, °C	A	L	IB[c]	IBD[c]
1	$(CD_3)_2CDOH$	0	25	0	0	0	0
2	$(CD_3)_2CDOH$	0	60	21[d]	0	1	3
3[e]	$(CD_3)_2CDOH$	0	60	0	0	0	0
4	$(CD_3)_2CDOH$	50	25	0	0	0	0
5	$(CD_3)_2CDOH$	50	60	25[d]	0	8	0
6	C_6D_6	0	25	0	0	0	0
7	C_6D_6	0	60	42[d]	0	1	0
8[e]	C_6D_6	0	60	5[d]	0	2	2
9	C_6D_6	50	25	0	0	0	0
10	C_6D_6	50	60	32[d]	0	0	4
11	THF-d_8	0	25	0	0	0	0
12	THF-d_8	0	60	63[d]	0	6	3
13[e]	THF-d_8	0	60	6[d]	0	6	0
14	THF-d_8	50	25	0	0	0	0
15	THF-d_8	50	60	55[d]	0	0	16
16[f]	hexane	0	25	0	0		
17[f]	hexane	0	60	41[d]	0		
18[e,f]	hexane	0	60	46[d]	0		
19[f]	hexane	50	25	0	0		
20[f]	hexane	50	60	41[d]	0		

[a]Conditions: [**A**] = [**L**] = 10 mM; 24 h. [b]Determined by the ^{1}H NMR analysis. [c]**IB** = isobutene, **IBD** = isobutene dimer (2,5-dimethylhexa-1,5-diene). [d]Black precipitate was observed. No ^{1}H NMR signal except for those of **A** and **L** was detected. [e]In the absence of **L**. [f]^{1}H NMR was measured in C_6D_6 after evaporation.

DOI: 10.1021/jacs.5b02350
J. Am. Chem. Soc. 2015, 137, 8138−8149

("Ru(0)") or a RuH cluster ("RuH"), was generated at an elevated temperature. Figure 5 shows the possible pathways

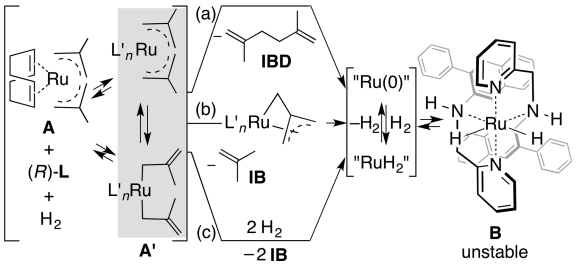

Figure 5. Supposed decomposition pathways from **A**, (*R*)-**L**, and H_2 to a black precipitate. **L**′ = cod, solvent, H_2, (*R*)-**L**, etc.; n = 1−4.

from **A**, (*R*)-**L**, and H_2 to the black precipitate. **A**′ is an imaginary bismethallyl species, in which cod of **A** is fully or partly replaced with solvent, H_2, (*R*)-**L**, etc. In route (a), coupling of the two methallyl ligands in **A** or **A**′ gives isobutene dimer (**IBD**), 2,5-dimethylhexa-1,5-diene, and "Ru(0)".[26] In route (b), **A** or **A**′ is converted to isobutene (**IB**) and a trimethylenemethane Ru(II) species,[27] which decomposes to "Ru(0)" via "RuH". In route (c), **A** or **A**′ directly reacts with H_2 to generate **IB** and "RuH",[25] which decomposes to "Ru(0)". In all routes, the decomposition may proceed via RuH_2((*R*)-**L**) (**B**).

In discussing the results shown in Table 1, care must be taken because (i) **IB** and **IBD** were not quantitatively detected and (ii) the ^{1}H NMR spectra tended to broaden. The black precipitate may absorb these alkenes to some extent, and aggregates of RuH species may be formed.[25,28] With such uncertainty in mind, the results were examined. In $(CD_3)_2CDOH$, which is the solvent of choice in the present asymmetric hydrogenation, no reaction of **A** with **L** occurred at 25 °C even after 24 h at 0 or 50 atm of H_2 (entries 1 and 4). An increase in temperature to 60 °C at 50 atm of H_2 decomposed 25% of **A** to generate a black precipitate together with 8% of **IB** (entry 5). Little **IBD** was detected, negating route (a). Removal of H_2 from the condition of entry 5 also led to a black precipitate, but, in this case, **IB** and **IBD** were generated in ca. 1:3 ratio (entry 2). Routes (a−c) may proceed in parallel. Interestingly, in the absence of **L**, nothing occurred (entries 2 and 3). The NH proton of **L** or association of **L** with **A** may accelerate the decomposition.[29] A basically similar tendency was observed in aprotic solvents such as C_6D_6 and THF-d_8 (entries 6−15) in terms of the black precipitate. Unlike the case with $(CD_3)_2CDOH$, however, **IBD** was detected at 50 atm of H_2 (entries 10 and 15). Routes (b) and (c) are suppressed in aprotic solvents for some reason. In hexane, **A** decomposed at 60 °C regardless of whether H_2 or **L** was present or not (entries 16−20).

Although the decomposition occurred only at an elevated temperature, the series of results in $(CD_3)_2CDOH$ are not inconsistent with the view that an infinitesimal amount of **B** is formed via hydrogenolysis of methallyl groups by two hydrogen molecules under the real hydrogenation conditions at 25 °C (see sections 2.4 and 2.5). As compared with the phosphorus atom-ligating RuH_2, **B**, which possesses electron-donating and non-π-acceptable sp^3N atoms trans to two hydrides, would be significantly destabilized to decompose without **AP**. Furthermore, replacement of cod in **A** would be more difficult with **L** than with the phosphorus-based ligand.

2.2.3. In Situ NMR Study. Figure 6 shows the ^{1}H NMR spectra of the reaction mixture before and after introduction of

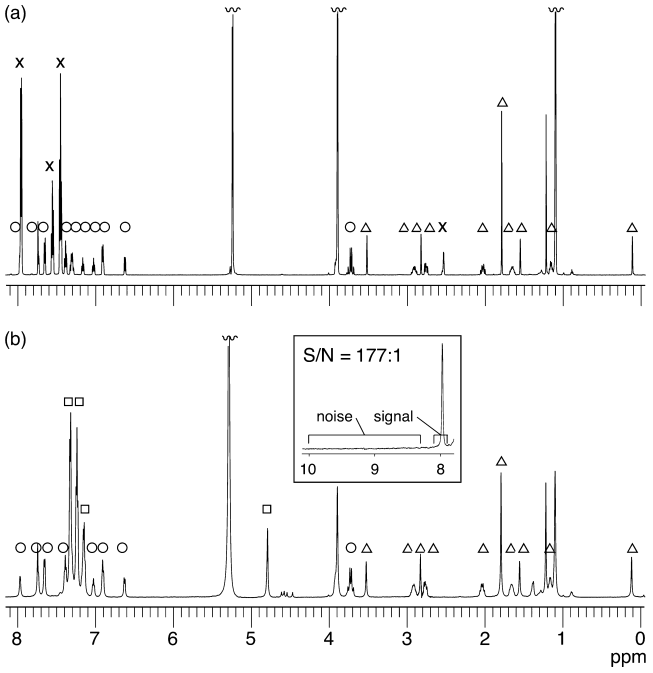

Figure 6. In situ ^{1}H NMR monitoring of the hydrogenation of acetophenone (**AP**, 75 mM) to 1-phenylethanol (**PE**) in $(CD_3)_2CDOD$ containing (*R*)-Ph-BINAN-H-Py ((*R*)-**L**, 10 mM), Ru(π-$CH_2C(CH_3)CH_2)_2$(cod) (**A**, 10 mM), and *t*BuOK (6.7 mM) at 25 °C. (a) Spectrum obtained 1.5 h after allowing the reaction mixture to stand without H_2. (b) Spectrum obtained 27 h after applying 50 atm of H_2 pressure to the reaction in (a) in a pressure-tight sapphire tube. The signal/noise ratio in spectrum (b) is calculated to be 177, as shown in the inset. The signals are indicated by ○ ((*R*)-**L**), △ (**A**), × (**AP**), and □ (**PE**).

H_2 ([(*R*)-**L**]$_0$ = [**A**]$_0$ = 10 mM, [*t*BuOK] = 6.7 mM, [**AP**]$_0$ = 75 mM, 50 atm H_2, $(CD_3)_2CDOD$, 25 °C, 27 h). In the ^{1}H NMR spectrum obtained 1.5 h after the addition of all components except for H_2 (Figure 6a), sets of signals corresponding to **A** (△), (*R*)-**L** (○), **AP** (×), and *t*BuOK were independently observed, although the CH_3 signal intensity of **AP** had decreased owing to hydrogen−deuterium (H/D) exchange via formation of the enolate of **AP**. After pressurizing the system to 50 atm of H_2, the **AP** signals (×) disappeared and the **PE** product signals (□) appeared, whereas there was no change in the signals of **A** or (*R*)-**L**. The *R*/*S* ratio of the **PE** product formed was 86:14. Within the limits of the signal-to-noise (S/N) ratio (177), no Ru−(*R*)-**L** complex formed. Nonetheless, we believe that a very tiny amount of a chiral and reactive species **B** ([**B**] < 10/177 mM = 0.0565 mM) is slowly generated under the hydrogenation conditions and is operating in this catalysis. **B** would survive only in the presence of the substrate **AP**.

2.3. Time−Conversion (*t*/[PE]) Curves. The time course of the IR C=O stretching band intensity of **AP** at 1690 cm^{-1} was obtained by use of a total internal reflectance measurement system during the hydrogenation of **AP** using the (*R*)-**L**/**A** combined catalyst under the standard conditions ([(*R*)-**L**]$_0$ = [**A**]$_0$ = [*t*BuOK] = 2 mM, [**AP**]$_0$ = 2 M, 50 atm H_2, *i*PrOH, 25 °C).[20] The data were converted to the *t*/[**PE**] curve shown in Figure 7a, together with those obtained at [**AP**]$_0$ = 0.5 and 1 M.

DOI: 10.1021/jacs.5b02350
J. Am. Chem. Soc. 2015, 137, 8138−8149

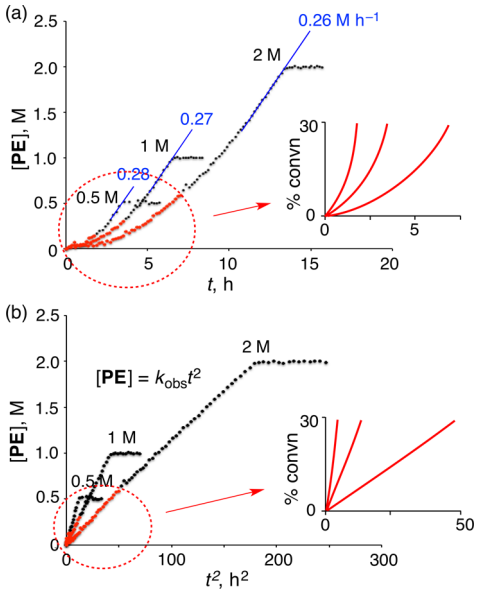

Figure 7. (a) Intriguing phenomenon observed in the t/[**PE**] relation at $[\mathbf{AP}]_0$ = 0.5, 1, and 2 M (conditions: [(*R*)-**L**] = [**A**] = [*t*BuOK] = 2 mM, 50 atm H_2, *i*PrOH, 25 °C). (b) Plot of [**PE**] versus t^2.

The following intriguing observations can be made from the three t/[**PE**] curves: (i) the velocity of **PE** production (d[**PE**]/dt) increases exponentially in the early stages but follows a rather straight relationship in the later stages; (ii) d[**PE**]/dt does not decelerate even at the very final stage; and (iii) d[**PE**]/dt decreases as $[\mathbf{AP}]_0$ increases. Observation (i) is not inconsistent with the scenario that the reactive species **B** is gradually generated during the course of the reaction, but it argues against the possible existence of an acceleration effect of product **PE**. The slight rate deceleration (0.28 M h^{-1} ($[\mathbf{AP}]_0$ = 0.5 M), 0.27 M h^{-1} (1 M), and 0.26 M h^{-1} (2 M)) in the straight line region of 70−100% conversion would instead indicate very weak product inhibition. Observation (ii) implies a zeroth-order dependence on **AP** concentration in the reaction system, while observation (iii) clearly shows that the reaction is inhibited by the initial concentration of **AP** ($[\mathbf{AP}]_0$). The difference between the reaction profile in the early stages and that in the later stages may be ascribed not only to the time-dependent change in [**AP**], [**PE**], and [**B**] but also to the decomposition of **B** at a lower concentration of **AP**. The rate is not enhanced as much as expected in the later stages, where the concentration of **B** increases. The balance between **B** generation and decomposition may result in observation (i). To simplify the subsequent discussion, *we will focus on the kinetic scheme of the present asymmetric hydrogenation only in the early stages (0−30% conversion of* ***AP****) of the reaction.*

2.4. Supposed Catalytic Cycle and Rate Law Analysis.

On the basis of the above experimental results and the mechanism reported for other Ru(II)-catalyzed hydrogenations,[21−24] we supposed the kinetic model shown in Figure 8, in which there are two processes occurring in parallel. One is the preliminary step with the rate constant k_0 from Ru(π-$CH_2C(CH_3)CH_2)_2$(cod) (**A**)/(*R*)-Ph-BINAN-H-Py ((*R*)-**L**)/H_2 to the reactive and unstable Λ-*cis*-α-**B** intermediate, and the other is the catalytic cycle itself for hydrogenation of **AP** to **PE** based on the Intramol-DACat mechanism (Figure 1b). In the absence of **AP**, the short-lived **B** easily decomposes by the liberation of **L**, while in the presence of **AP**, the polarized $H^{\delta+}$−$N^{\delta-}$---$Ru^{\delta+}$−$H^{\delta-}$ moiety of the 18e Ru dihydride **B** captures the similarly polarized $C^{\delta+}$═$O^{\delta-}$ of **AP** to move to transition state **C**. In this charge-alternating six-atom system, the red and blue hydrogen atoms are delivered to the C═O double bond to release **PE** together with generation of the 16e Ru amide **D**, which would have a trigonal bipyramidal structure with a Ru═N double-bond character.[21c] The coordinatively unsaturated **D** interacts with H_2 in an η^2 manner to form **F**, which undergoes heterolytic cleavage to reproduce the chain carrier **B**, thereby completing the catalytic cycle. The rate of the cycle would be determined by the **D** −> **B** step with k_2 and not by the **B** −> **D** step with k_1 ($k_2 \ll k_1$).[21c] The Ru amide **D** interacts not only with H_2 but also with **AP**, **PE**, and *i*PrOH to form equilibria with the corresponding Ru enolate and Ru alkoxide $\mathbf{E}_{\mathbf{QH}}$ and the equilibrium constant K_{QH}, thereby causing inhibition.[21f,23c]

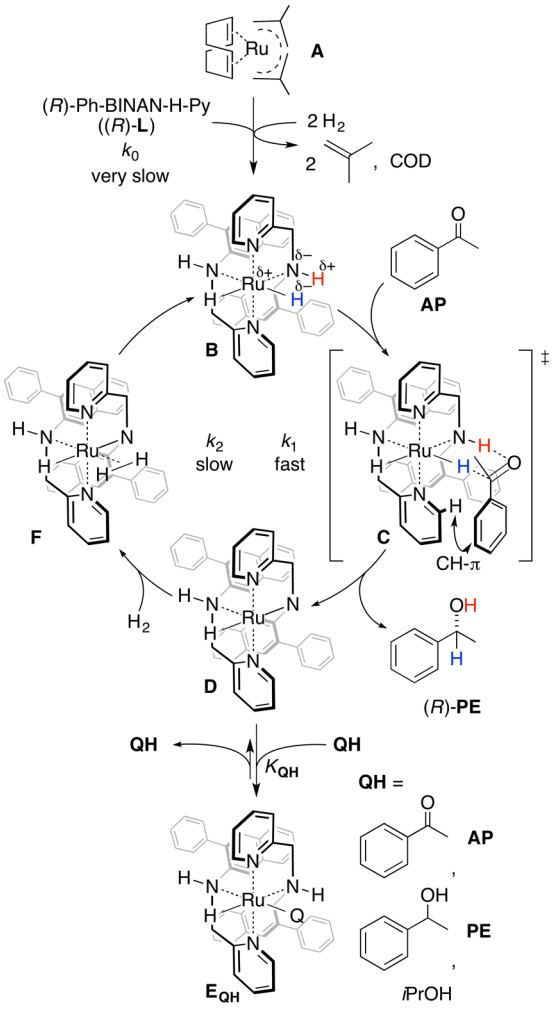

Figure 8. Reaction pathway and enantioface selection in the Intramol-DACat-based hydrogenation of acetophenone (**AP**) using (*R*)-Ph-BINAN-H-Py ((*R*)-**L**) and Ru(π-$CH_2C(CH_3)CH_2)_2$(cod) (**A**).

In the present particular case, the catalyst precursor **A** is consumed by the action of H_2 and **L** to generate **B** with an extraordinarily slow rate on the time scale of hydrogenation, enabling [**A**] and [**L**] to be approximated by $[\mathbf{A}]_0$ and $[\mathbf{L}]_0$, respectively ([**A**] ≈ $[\mathbf{A}]_0$ and [**L**] ≈ $[\mathbf{L}]_0$). Hydrogen pressure ($[H_2]$) and *t*BuOK concentration ([*t*BuOK]) do not change during the reaction. Therefore, the total concentration of the Ru species in the cycle ($[Ru_{cycle}]$) can be expressed as $k_0[\mathbf{A}]_0^l[\mathbf{L}]_0^m[H_2]^n t$.[20] Furthermore, under the condition of k_2

DOI: 10.1021/jacs.5b02350
J. Am. Chem. Soc. 2015, 137, 8138−8149

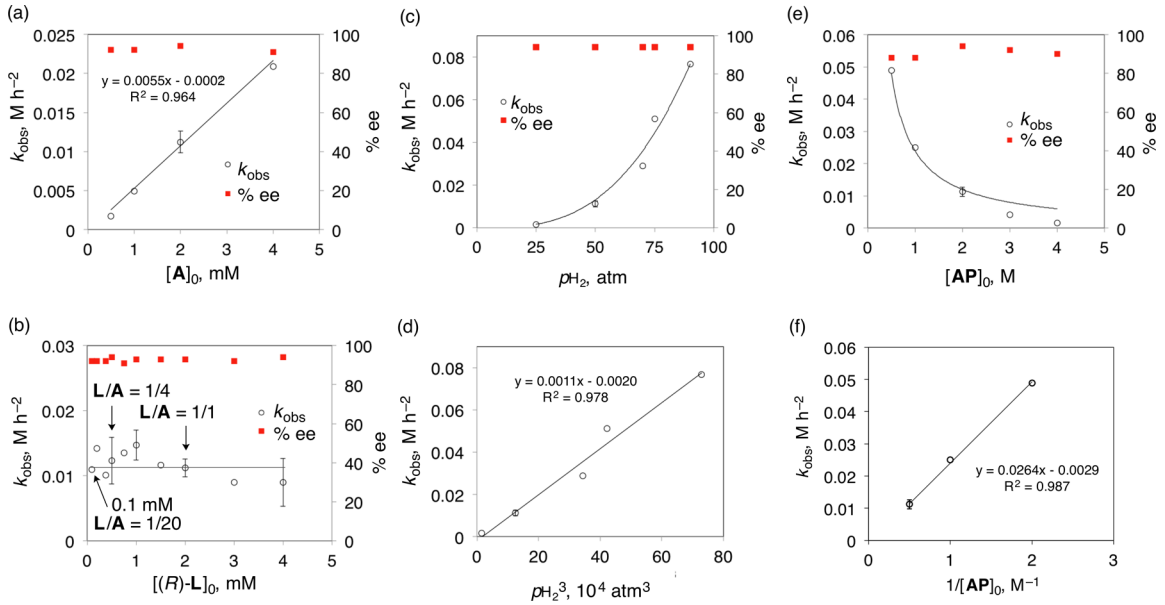

Figure 9. Dependence of the rate constant k_{obs} on [Ru(π-CH$_2$C(CH$_3$)CH$_2$)$_2$(cod) (**A**)]$_0$, [(*R*)-Ph-BINAN-H-Py ((*R*)-**L**)]$_0$, H$_2$ pressure (pH$_2$), and [acetophenone (**AP**)]$_0$ in the hydrogenation of **AP** in *i*PrOH at 25 °C. (a) Plot of k_{obs} as a function of [**A**]$_0$ from 0.5 to 4 mM ([(*R*)-**L**]$_0$ = [*t*BuOK] = 2 mM, [**AP**]$_0$ = 2 M, 50 atm H$_2$). (b) Plot of k_{obs} as a function of [(*R*)-**L**]$_0$ from 0.1 to 4 mM ([**A**]$_0$ = [*t*BuOK] = 2 mM, [**AP**]$_0$ = 2 M, 50 atm H$_2$). (c) Plot of k_{obs} as a function of pH$_2$ from 25 to 90 atm ([**A**]$_0$ = [(*R*)-**L**]$_0$ = [*t*BuOK] = 2 mM, [**AP**]$_0$ = 2 M). (d) Plot of k_{obs} as a function of pH$_2$^{3} of graph (c). (e) Plot of k_{obs} as a function of [**AP**]$_0$ from 0.5 to 4 M ([**A**]$_0$ = [(*R*)-**L**]$_0$ = [*t*BuOK] = 2 mM, 50 atm H$_2$). (f) Plot of k_{obs} as a function of 1/[**AP**]$_0$ of graph (e).

$\ll k_1$, the Ru$_{cycle}$ is distributed mainly to **D** and **E**$_{QH}$ ([Ru$_{cycle}$] = [**D**] + Σ[**E**$_{QH}$] = [**D**](1 + ΣK_{QH}[**QH**])), leading to eq 1.

$$[\mathbf{D}] = k_0[\mathbf{A}]_0^{\,l}[\mathbf{L}]_0^{\,m}[\mathrm{H_2}]^n t/(1 + \sum K_{\mathbf{QH}}[\mathbf{QH}]) \quad (1)$$

Steady-state assumption for **D** gives d[**PE**]/dt = k_2[**D**][H$_2$] = k_0k_2[**A**]$_0^{\,l}$[**L**]$_0^{\,m}$[H$_2$]^{n+1}t /(1 + ΣK_{QH}[**QH**]). With the definitions of ΣK_{QH}[**QH**] = $K_{\mathbf{AP}}$[**AP**] + $K_{(R)\text{-}\mathbf{PE}}$[(*R*)-**PE**] + $K_{(S)\text{-}\mathbf{PE}}$[(*S*)-**PE**] + $K_{i\mathrm{PrOH}}$[*i*PrOH] and $K_{\mathbf{PE}}$[**PE**] = $K_{(R)\text{-}\mathbf{PE}}$[(*R*)-**PE**] + $K_{(S)\text{-}\mathbf{PE}}$[(*S*)-**PE**] = $ZK_{\mathbf{AP}}$[**PE**], integration of the d[**PE**]/dt equation from 0 to t followed by the second-order Taylor expansion at t = 0 gives eq 2.[20]

$$[\mathbf{PE}] = (k_0k_2[\mathbf{A}]_0^{\,l}[\mathbf{L}]_0^{\,m}[\mathrm{H_2}]^{n+1}/2(K_{\mathbf{AP}}[\mathbf{AP}]_0 + K_{i\mathrm{PrOH}}[i\mathrm{PrOH}] + 1))t^2 = k_{obs}t^2 \quad (2)$$

Consistent with eq 2, time-squared plotting of the t/[**PE**] relations in Figure 7a gave straight lines, at least in the early reaction stages (Figure 7b), implying that the preliminary step from (*R*)-**L**/**A**/H$_2$ to **B** and the catalytic cycle converting **AP** to **PE** are operating in parallel.

2.5. Reaction Orders for [A]$_0$, [L]$_0$, [H$_2$] (pH$_2$), and [AP]$_0$. The time-squared equation, [**PE**] = $k_{obs}t^2$, was used to deduce the reaction orders for **A**, (*R*)-**L**, pH$_2$, and **AP**. The values of k_{obs} in all of the kinetic experiments were derived by using data obtained at the initial stages of the reaction, between 0% and 30% conversion, where the linearity is the highest (Figure 7b, red line).[20] The relationship between k_{obs} and each parameter is shown in Figure 9a–f.

The plots of k_{obs} versus [**A**]$_0$ from 0.5 to 4 mM gave a reasonably linear relationship from the origin with a correlation coefficient of 0.964, indicating a first-order dependence on [**A**]$_0$ (l = 1 in eq 2) (Figure 9a). The rate was essentially not affected by [**L**]$_0$ (0.1–4 mM) (m = 0 in eq 2) within the range of error distribution (Figure 9b). The k_{obs} value exponentially increases as pH$_2$ increases from 25 to 90 atm (Figure 9c) according to an accurate cubic function. Figure 9d shows a third-order plot affording a straight line from the origin with a correlation coefficient of 0.978, establishing n + 1 = 3 in eq 2. In contrast to the acceleration effect of pH$_2$ on the rate, the k_{obs} value exponentially decreases as [**AP**]$_0$ increases from 0.5 to 4 M (Figure 9e). Replotting the k_{obs} values versus the reciprocal of [**AP**]$_0$ established a reasonable linearity with a correlation coefficient of 0.987 (Figure 9f). The −1st-order dependence on [**AP**]$_0$ is consistent with eq 2. The rates observed with [**AP**]$_0$ at 3 and 4 M were rather slower than those expected from the 0.5–2 M data. This deviation is probably due to changes in the properties of the solvent, which comprises *i*PrOH and **AP** in a 2:1 to 1:1 ratio, because the characteristics of **AP** exert a significant effect on the polarity and dielectronic constant of the solvent system.[23d] In all cases, the high enantioselectivity was maintained with [**A**]$_0$, [**L**]$_0$, pH$_2$, and [**AP**]$_0$ varied (Figure 9, red squares).

Equation 2 can therefore be rewritten as eq 3.

$$[\mathbf{PE}] = (k_0k_2[\mathbf{A}]_0[H_2]^3/2(K_{\mathbf{AP}}[\mathbf{AP}]_0 + K_{i\mathrm{PrOH}}[i\mathrm{PrOH}] + 1))t^2 = k_{obs}t^2 \quad (3)$$

2.6. Inhibitory Effect. Equation 3 applies only in the early stages of the reaction; therefore, no [**PE**] term is included. Inhibition of the catalytic activity, however, should be related to all possible **QH** species, including substrate **AP**, product **PE**, and solvent *i*PrOH, in the equilibrium **D** + **QH** $\rightleftarrows$ **E**$_{QH}$ with K_{QH} in Figure 8. Formation of the Ru enolate and alkoxide as **E**$_{QH}$ is the most probable inhibitory process,[21f,23c] and the order of the inhibitory effect is thought to be **AP** > **PE** > *i*PrOH based on the pKa (H$_2$O) values (**AP** enol (10.34),[30] **PE** (15.4),[31] and *i*PrOH (16.5)[32]). The inhibitory factor is not simple, being affected not only by acid and base principles but also by the concentration, steric and electronic properties of **E**$_{QH}$, and the emergence of other reaction pathways specific to **E**$_{QH}$.

DOI: 10.1021/jacs.5b02350
J. Am. Chem. Soc. 2015, 137, 8138–8149

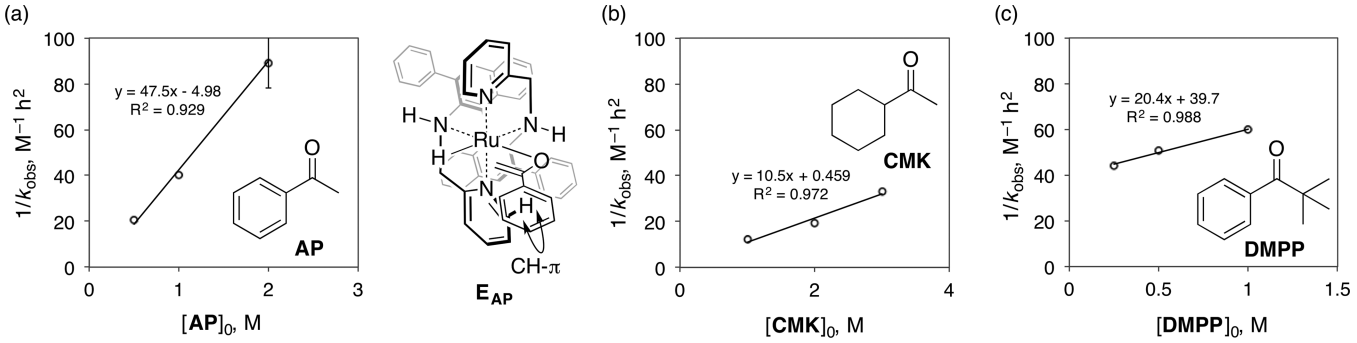

Figure 10. Comparison of the inhibitory effect of acetophenone (**AP**), cyclohexyl methyl ketone (**CMK**), and 2,2-dimethylpropiophenone (**DMPP**) under the standard conditions ($[(R)$-Ph-BINAN-H-Py $((R)$-**L**$)]_0 = [\mathrm{Ru}(\pi\text{-}CH_2C(CH_3)CH_2)_2(\mathrm{cod})$ (**A**$)]_0 = [t\mathrm{BuOK}] = 2$ mM, 50 atm H_2, *i*PrOH, 25 °C). (a) Reciprocal plot of k_{obs} versus $[\mathbf{AP}]_0$. (b) Reciprocal plot of k_{obs} versus $[\mathbf{CMK}]_0$. (c) Reciprocal plot of k_{obs} versus $[\mathbf{DMPP}]_0$. In (a), (b), and (c), the slope corresponds to $2(K_{\mathbf{QH}}[\mathbf{QH}]_0 + K_{i\mathrm{PrOH}}[i\mathrm{PrOH}] + 1)/k_0k_2[\mathbf{A}]_0[\mathrm{H_2}]^3$ (**QH** = **AP**, **CMK**, or **DMPP**). Because the value of the denominator is constant under a given condition, a steeper slope means greater inhibition.

To make a qualitative interpretation of the inhibitory effect, the following experiments were carried out by using **AP**, cyclohexyl methyl ketone (**CMK**), 2,2-dimethylpropiophenone (**DMPP**), (R)-**PE**, and (S)-**PE**: **CMK** is enolizable but lacks the benzene ring of **AP**, whereas **DMPP** is not enolizable but has a benzene ring. (R)-**PE** is the major product of (R)-**L**/**A**-catalyzed asymmetric hydrogenation, while (S)-**PE** is the minor enantiomeric product. In comparing inhibition among **AP**, **CMK**, and **DMPP**, however, care must be taken because these ketones are completely different both sterically and electronically and vary in reactivity and selectivity in the (R)-**L**/**A**-catalyzed asymmetric hydrogenation: namely, 94:6 er and $k_{obs} = 2.50 \times 10^{-2}$ M h^{-2} for **AP**; 42:58 er and $k_{obs} = 8.31 \times 10^{-2}$ M h^{-2} for **CMK**; and 93:7 er and $k_{obs} = 1.67 \times 10^{-2}$ M h^{-2} for **DMPP** at a substrate concentration of 1 M. Bearing this in mind, and with the assumption that the same mechanism is operating as for **AP**, the inhibitory effect was investigated as discussed below.

*2.6.1. Ketone Substrates: **AP**, **CMK**, and **DMPP**.* To analyze the inhibitory effect of ketone substrates and *i*PrOH, eq 3 was converted to eq 4.

$$1/k_{obs} = 2(K_{\mathbf{AP}}[\mathbf{AP}]_0 + K_{i\mathrm{PrOH}}[i\mathrm{PrOH}] + 1) /k_0k_2[\mathbf{A}]_0[\mathrm{H_2}]^3 \quad (4)$$

The plots of $1/k_{obs}$ versus $[\mathbf{AP}]_0$ gave a straight line with a small *y*-intercept value (−4.98) within the range of 0.5−2 M (Figure 10a). The direct proportion from the origin shows that (i) **AP** is the major inhibitor of the formation of **D**; (ii) the **D** ⇄ $\mathbf{E_{AP}}$ equilibrium point lies toward the far $\mathbf{E_{AP}}$ side ($1 \ll K_{\mathbf{AP}}$); and (iii) inhibition by *i*PrOH is negligible ($K_{i\mathrm{PrOH}} \ll K_{\mathbf{AP}}$). The inhibition profile of **CMK** also showed the same tendency as that of **AP** (Figure 10b), albeit with a 4.5-fold shallower slope than **AP** (47.5 vs 10.5). We assume that this difference may originate from CH-π stabilization of $\mathbf{E_{AP}}$, whereby the C_6H_5 π system interacts with the PyC(6)H of the Ph-BINAN-H-Py ligand. The extra inhibitory factor exists only for **AP** and not for **CMK**, reflecting the lower reactivity of **AP** ($k_{obs} = 2.50 \times 10^{-2}$ M h^{-2} for $[\mathbf{AP}]_0 = 1$ M; $k_{obs} = 8.31 \times 10^{-2}$ M h^{-2} for $[\mathbf{CMK}]_0 = 1$ M). By contrast, **DMPP**, which has no proton, gave a straight line with a shallow slope (20.4) and a large *y*-intercept (+39.7) as shown in Figure 10c. This profile can be understood by assuming that nonenolizable **DMPP** relatively enhances the degree of the *i*PrOH inhibitory effect toward the catalytic cycle via a 16e Ru amide **D**. Nonetheless, because **DMPP** causes little inhibition in the present catalysis, it shows less reactivity than **AP** ($k_{obs} = 1.67 \times 10^{-2}$ vs 2.50×10^{-2} M h^{-2}). A steric effect of **DMPP** would be the reason.

This series of experiments indicates that the inhibition resulting from **AP** and **CMK** would be caused mainly by formation of the Ru *O*-enolate[21f,33] and partly by the phenyl group of **AP**. In addition, the reaction of **AP** at 1 M was not inhibited by the addition of ethylbenzene in the range of 1−2 M under the standard conditions.[20] This result supports the idea that the major inhibitory factor of **AP** originates from formation of the CH-π-stabilized Ru *O*-enolate $\mathbf{E_{AP}}$ and not from the arene−Ru complex.

2.6.2. Enantiomeric Products: (R)-PE and (S)-PE. To evaluate the inhibitory effect of **PE** quantitatively, reaction rates were determined for the hydrogenation of **AP** (0.5 M) under the standard conditions except for the presence of 0.5 and 1 M **PE**. By defining the externally added (R)-**PE** and (S)-**PE** as (R)-$\mathbf{PE_{ex}}$ and (S)-$\mathbf{PE_{ex}}$, respectively, eq 5 can be deduced.[20]

$$1/k_{obs} = 2(K_{\mathbf{AP}}[\mathbf{AP}]_0 + K_{(R)\text{-}\mathbf{PE}}[(R)\text{-}\mathbf{PE_{ex}}] + K_{(S)\text{-}\mathbf{PE}}[(S)\text{-}\mathbf{PE_{ex}}] + K_{i\mathrm{PrOH}}[i\mathrm{PrOH}] + 1) /k_0k_2[\mathbf{A}]_0[\mathrm{H_2}]^3 \quad (5)$$

Because $1/k_{obs}$ shows a linear relation to both $[(R)$-$\mathbf{PE_{ex}}]$ and $[(S)$-$\mathbf{PE_{ex}}]$ in eq 5, the slope in the plots of $1/k_{obs}$ against $[\mathbf{PE_{ex}}]$ indicates the degree of the inhibitory effect. As shown in Figure 11a, the product (R)-**PE**, which is generated from (R)-**L**/**A** catalysis, had little effect on the reactivity, giving a shallow slope. By contrast, the enantiomeric product (S)-**PE**, which is the minor product in the present *R* catalysis, significantly inhibited the reaction. The $K_{(S)\text{-}\mathbf{PE}}/K_{(R)\text{-}\mathbf{PE}}$ ratio approached 15 (slope ratio = 176/12). The 15-fold difference in the equilibrium constant may be due to a CH-π interaction between the phenyl group of (S)-**PE** alkoxide and PyC(6)H of (R)-**L**, which would stabilize $\mathbf{E}_{(S)\text{-}\mathbf{PE}}$.[34] The conformer with such a CH-π interaction in the corresponding Ru−(R)-**PE** alkoxide ($\mathbf{E}_{(R)\text{-}\mathbf{PE}}$) would be energetically unfavored for steric reasons. The methyl group is forced into a location in the crowded region (see Figure 11, upper structure). These results imply that chiral amplification may occur in the present asymmetric hydrogenation via a new mechanism.[7b,35]

2.7. Simulation. A series of kinetic studies revealed that the present asymmetric hydrogenation of **AP** proceeds without

DOI: 10.1021/jacs.5b02350
J. Am. Chem. Soc. 2015, 137, 8138−8149

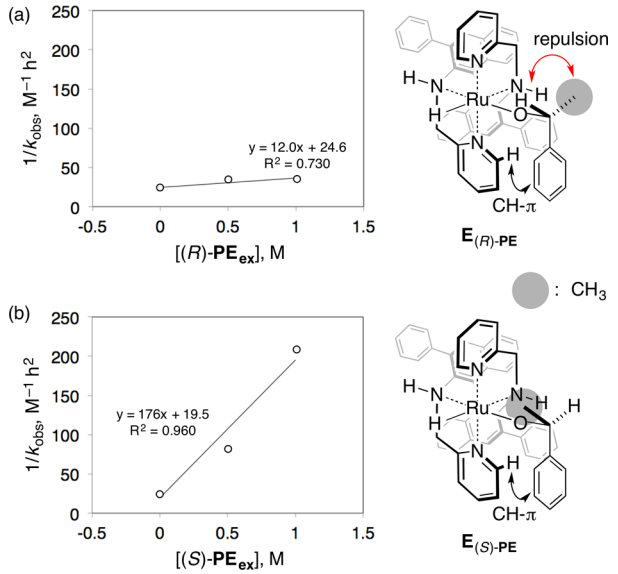

Figure 11. Quantitative analysis of the inhibitory effect of (*R*)-1-phenylethanol ((*R*)-**PE**) and (*S*)-**PE**, and possible structures of the Ru alkoxides, $\mathbf{E}_{(R)\text{-PE}}$ and $\mathbf{E}_{(S)\text{-PE}}$. (a) Reciprocal plot of k_{obs} versus [(*R*)-$\mathbf{PE}_{ex}$]. (b) Reciprocal plot of k_{obs} versus [(*S*)-$\mathbf{PE}_{ex}$]. Hydrogenation of **AP** (0.5 M) was carried out in the absence and presence of **PE** (0.5 and 1 M) under the standard conditions ([(*R*)-Ph-BINAN-H-Py ((*R*)-**L**)]$_0$ = [Ru(*π*-$CH_2C(CH_3)CH_2)_2$(cod) (**A**)]$_0$ = [*t*BuOK] = 2 mM, 50 atm H_2, *i*PrOH, 25 °C). The red arrow indicates a steric repulsion.

significant inhibition from the solvent *i*PrOH and the major product (*R*)-**PE**; therefore, the kinetic profile shown in Figure 8 can be expressed by eq 6 in the early stages of the reaction under the standard conditions.

$$[\mathbf{PE}] = k_{obs}t^2 = k_0k_2[\mathbf{A}]_0[H_2]^3t^2/2K_{\mathbf{AP}}[\mathbf{AP}]_0 \quad (6)$$

To confirm its validity, eq 6 was used to simulate the relationships between time and **PE** concentration, which were then compared with the *t*/[**PE**] curves observed under different conditions of [**A**]$_0$, pressure pH_2, or [**AP**]$_0$. The k_{obs} values obtained under the conditions of [**A**]$_0$ = 1−4 mM, pH_2 = 25−90 atm, and [**AP**]$_0$ = 0.5−2 M (Figure 9a, c, and e) gave $k_0k_2/K_{\mathbf{AP}}$ = 4.1 × 10^3 M^{-2} h^{-2} as the average value.[36] This value was substituted into eq 6 to simulate the *t*/[**PE**] relationship (Figure 12a−c). Close agreement between the simulated (blue surfaces) and experimental (red lines) curves confirmed that the hydrogenation proceeds according to eq 6 with a $k_0k_2/K_{\mathbf{AP}}$ value of 4.1 × 10^3 M^{-2} h^{-2} in the early stages.

2.8. Effect of [L]$_0$ and [*t*BuOK]. As shown in Figure 9b, the initial concentration of (*R*)-**L** in the range of 0.1−4 mM has little effect on the rate. Therefore, even a reaction with a smaller amount of **L** than **A** ([**L**]$_0$ = 0.5 mM; [**A**]$_0$ = 2 mM; **L**/**A** = 1/4) showed essentially the same reactivity and selectivity as that with an **L**/**A** ratio of 1:1. Moreover, a further decrease in the **L**/**A** ratio to 1/20 ([**L**]$_0$ = 0.1 mM; [**A**]$_0$ = 2 mM) produced **PE** in an *R*/*S* er of 96:4 without a significant loss of reactivity. As shown in Figure 13, an even further decrease in the **L**/**A** ratio

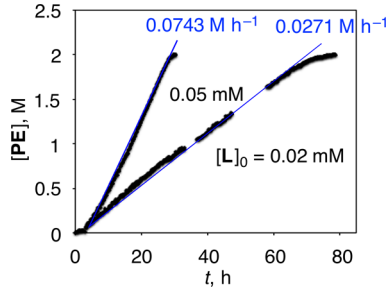

Figure 13. Time−product concentration curves obtained with an extremely low concentration of (*R*)-**L** ([**L**]$_0$ = 0.02 mM and 0.05 mM, [**A**]$_0$ = [*t*BuOK] = 2 mM, [**AP**]$_0$ = 2 M, 50 atm H_2).

to 1/40 ([**L**]$_0$ = 0.05 mM; [**A**]$_0$ = 2 mM) led to a straight line in terms of the *t*/[**PE**] relationship to the point of the reaction completion, giving (*R*)-**PE** with a 94:6 er. In the **L**/**A** ratio of 1/100 ([**L**]$_0$ = 0.02 mM and [**A**]$_0$ = 2 mM), the straight-line phenomenon was observed. Although the enantioselectivity decreased to 87:13, the degree of chiral multiplication approached 87 000. Under these conditions, the *t*/[**PE**] curve no longer follows the time-squared equation ([**PE**] = $k_{obs}t^2$). At such an extremely low concentration of **L**, all Ph-BINAN-H-Py molecules would be used to generate **B**. Consistent with this view, the rate of [**L**]$_0$ = 0.02 mM was proportionally slowed to 2/5 that of [**L**]$_0$ = 0.05 mM (0.0271 vs 0.0743 M h^{-1}). The rate of 0.26 M h^{-1} in the later stages under the standard conditions (Figure 7a) determines the approximate concentration of Ru_{cycle} to be 0.1−0.2 mM, supporting the fact that the rate is essentially not affected by [**L**]$_0$ > 0.1 mM (Figure 9b).

Within the range of 1−20 mM, the initial concentration of *t*BuOK was also not influential on the rate and enantioselectivity (Figure 14a). A concentration of *t*BuOK (1 mM) that was 50% lower than that of the Ru *π*-allyl precursor **A** (2 mM)

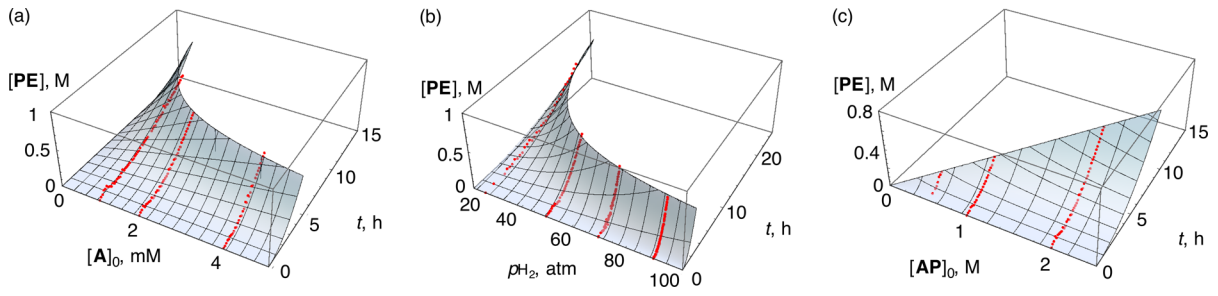

Figure 12. Simulation (blue surfaces) and observation (red lines) of the *t*/[**PE**] relationship from 0% to 30% conversion in the (*R*)-**L**/**A**-catalyzed hydrogenation of **AP** in *i*PrOH at 25 °C. (a) *t*/[**PE**] relationship as a function of [**A**]$_0$ ([(*R*)-**L**]$_0$ = [*t*BuOK] = 2 mM; [**A**]$_0$ = 1, 2, and 4 mM; [**AP**]$_0$ = 2 M; 50 atm H_2). (b) *t*/[**PE**] relationship as a function of pH_2 ([(*R*)-**L**]$_0$ = [**A**]$_0$ = [*t*BuOK] = 2 mM; [**AP**]$_0$ = 2 M; 25, 50, 70, and 90 atm H_2). (c) *t*/[**PE**] relationship as a function of [**AP**]$_0$ ([(*R*)-**L**]$_0$ = [**A**]$_0$ = [*t*BuOK] = 2 mM; [**AP**]$_0$ = 0.5, 1, and 2 M; 50 atm H_2). Simulation conditions: [**PE**] = $k_0k_2[\mathbf{A}]_0[H_2]^3t^2/2K_{\mathbf{AP}}[\mathbf{AP}]_0$ with $k_0k_2/K_{\mathbf{AP}}$ = 4.1 × 10^3 M^{-2} h^{-2}.

DOI: 10.1021/jacs.5b02350
J. Am. Chem. Soc. 2015, 137, 8138−8149

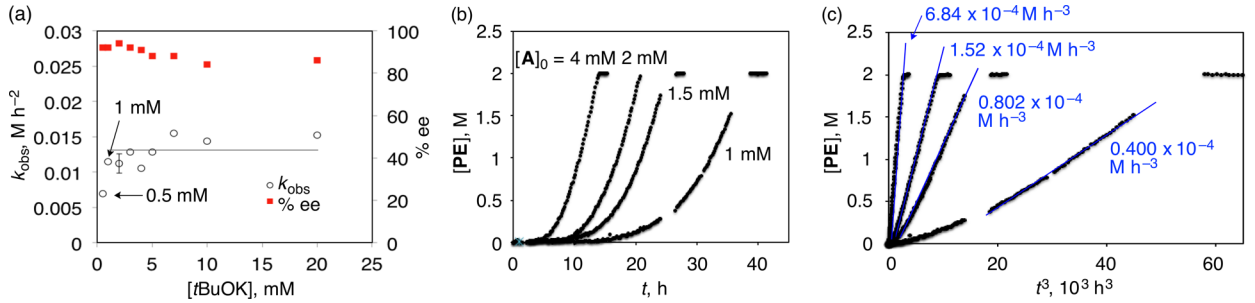

Figure 14. (a) Plot of k_{obs} as a function of [*t*BuOK] from 0.5 to 20 mM ([**A**]$_0$ = [(*R*)-**L**]$_0$ = 2 mM, [**AP**]$_0$ = 2 M, 50 atm H_2). (b) Time−product concentration curves obtained without *t*BuOK ([*t*BuOK] = 0 mM; [**L**]$_0$ = 2 mM; [**A**]$_0$ = 1, 1.5, 2, and 4 mM; [**AP**]$_0$ = 2 M; 50 atm H_2). (c) Plot of [**PE**] as a function of t^3 of graph (b).

was enough to maintain reactivity. When [*t*BuOK] was decreased to 0.5 mM, the reactivity was halved (k_{obs} = 1.17 × 10^{-2} vs 6.89 × 10^{-3} M h^{-2}). Furthermore, as shown in Figure 14b, even in the absence of *t*BuOK ([**A**]$_0$ = 1, 1.5, 2, and 4 mM), the reaction went to completion, although the rate was extremely slow in the early stages. Replotting the *t*/[**PE**] relation in Figure 14b as a function of t^3 exhibited a reasonably linear relationship (Figure 14c), although the t^3/[**PE**] curve obtained with [**A**]$_0$ = 1 mM deviated from the ideal one. The change in the order of *t* from second to third in the absence of [*t*BuOK] implies that the ever-changing species [Ru$_{cycle}$], [**AP**], and [**PE**] are involved in this cycle in a different way than when [*t*BuOK] is present under the standard conditions. The slopes of the linear lines in the t^3/[**PE**] plotting (blue lines) have a second-order dependence on [**A**]$_0$. So, when [**A**]$_0$ is increased from 1 to 1.5 mM, the slope is steeper by a factor of (1.5/1)^2 = 2.25, which is close to the observed value, (0.80 × 10^{-4})/(0.40 × 10^{-4}) = 2. The second-order dependence on [**A**]$_0$ can be also observed when 1.5 mM is increased to 2 mM ((2/1.5)^2 = 1.78 vs (1.52 × 10^{-4})/(0.80 × 10^{-4}) = 1.9), and when 2 mM => 4 mM ((4/2)^2 = 4 vs (6.84 × 10^{-4})/(1.52 × 10^{-4}) = 4.5). One possible explanation is that two Ru$_{cycle}$ molecules are involved in the catalytic cycle established in the absence of *t*BuOK. One Ru$_{cycle}$ species may act as a base instead of *t*BuOK. [Ru$_{cycle}$] increases with a first-order time dependence; as a result, the involvement of another Ru$_{cycle}$ in the cycle would alter [**PE**] = $k_{obs}t^2$ to [**PE**] = $k_{obs}t^3$. The inclusion of at least 1 mM *t*BuOK might prevent the aggregation of intermediary Ru species leading to **B**, or it might enhance the reactivity of **A** toward H_2, thereby initiating the reaction without an induction period.

2.9. Enantioface Selection. Figure 15 shows the **B** + **AP** −> **D** + **PE** step in detail. We believe that the reaction proceeds via the prior formation of an N−H---O=C hydrogen bond between **B** and **AP**. A clockwise rotation[37] of the C=O axis forms the transition state **C**$_{Si}$, in which the *Si* face of the electrophilic C=O group is facing the nucleophilic Ru hydrogen atom. An anticlockwise rotation[37] gives **C**$_{Re}$, the structure of which is sterically more favored than that of **C**$_{Si}$. Nevertheless, **C**$_{Si}$ is more favored than **C**$_{Re}$, resulting in the production of (*R*)-**PE** as the major product. This sense of enantioselectivity holds for various aromatic ketones.[13] An attractive interaction is expected to stabilize the **C**$_{Si}$ transition state: possible candidates would be (i) a CH-π interaction between PyC(6)H and the aromatic π system of **AP** (factor I) and (ii) a CH-π interaction between *ortho*-HPh of **AP** and the C(3)-,C(3′)-Ph π system of (*R*)-**L** (factor II).

2.9.1. Hammett Analysis. To determine which of these factors is involved, we examined the enantioselectivity of **AP**

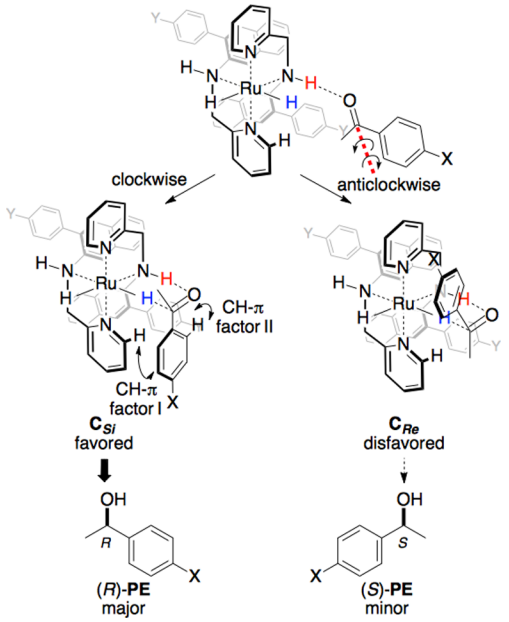

Figure 15. Proposed mechanism of enantioselection in the (*R*)-Ph-BINAN-H-Py−RuH$_2$-catalyzed hydrogenation of **AP**.

possessing a different ring substituent X at the para position, including CH_3O, CH_3, and CF_3.[20] All of the reactions were completed within 18 h under the standard conditions. The presence of an electron-donating substituent tended to increase the enantioselectivity, which ranged from an *R*/*S* er of 90:10 (4-CF_3) to an *R*/*S* er of 99:1 (4-CH_3O). The Hammett plot of ln(*R*/*S*) versus the standard σ constants for the substituent parameter exhibited a reasonably linear relationship (Figure 16a), indicating that a single reactive mechanism is operating in the asymmetric hydrogenation with the involvement of factor I. By contrast, the enantioselectivity with (*R*)-Ph-BINAN-H-Py ligands possessing a substituent Y at the para position of the C(3)-,C(3′)-phenyl group virtually remained unchanged (*R*/*S* er = 96:4−97:3) (Figure 16b). Overall, the transition state **C**$_{Si}$ is most likely to be stabilized by factor I: namely, a CH-π interaction between PyC(6)H and the aromatic π system of **AP**. This is the origin of the enantioselectivity in the (*R*)-**L**/**A**-catalyzed hydrogenation of **AP** giving (*R*)-**PE**.

2.9.2. $^{12}C/^{13}C$ Kinetic Isotope Effect. In this **B** −> **D** step, the hydrogen bond formation between **B** and **AP** would have no energy barrier, and the rate would be determined by the hydride transfer step via **C**$_{Si}$, where the blue-colored hydrogen atom on Ru and the red-colored hydrogen atom on sp^{3}N are delivered to the C=O bond in a concerted manner (see Figure

DOI: 10.1021/jacs.5b02350
J. Am. Chem. Soc. 2015, 137, 8138−8149

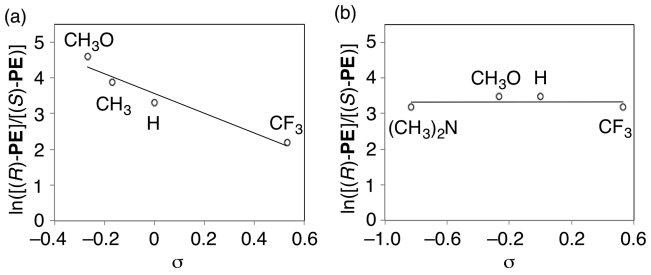

Figure 16. Hammett plots of ln([(*R*)-**PE**]/[(*S*)-**PE**]) as a function of standard σ constants. (a) Effect of substituent X at the para position of **AP** on enantioselectivity. (b) Effect of substituent Y at the para position of the Ph group of (*R*)-Ph-BINAN-H-Py on enantioselectivity.

15). Direct attack of RuH on C═O without formation of an sp^3N−H---O═C hydrogen bond is the most unlikely possibility.

To confirm the occurrence of Intramol-DACat-based hydride transfer, the $^{12}C/^{13}C$ isotope effect was measured.[20] The catalytic hydrogenation of **AP** was conducted on a 50 mmol scale under the standard conditions, and the reaction was stopped at 93% conversion (13 h). The reaction mixture was concentrated and subjected to silica gel column chromatography, which gave **PE** with an *R*/*S* er of 97:3 and **AP** (421 mg) in 6.9% yield. The recovered **AP** was subjected to ^{13}C NMR measurement, whereby the ^{13}C signal intensities were compared by using the ^{13}C signal at C_{para} of the phenyl group of **AP** (not involved in the reaction) as an internal standard. The relative proportion of the ^{13}C isotopic composition at C(1)═O was increased by 8.4% (Figure 17a). No other signals showed significant changes in ^{13}C

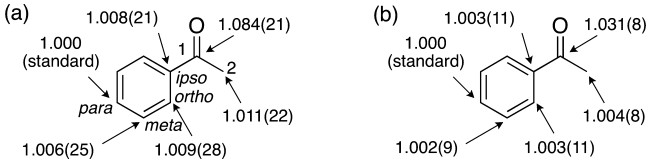

Figure 17. Measurement of the $^{12}C/^{13}C$ isotope effect in acetophenone (**AP**) recovered in 6.9% yield after 93% conversion to **PE** under the standard conditions. (a) ^{13}C isotopic composition determined by ^{13}C NMR analysis. (b) $^{12}C/^{13}C$ kinetic isotope effect calculated by using C_{para} as a standard.

isotopic composition. Using the equations of Singleton and Thomas,[38] the $^{12}C/^{13}C$ isotope effect was calculated to be 1.031 (Figure 17b). This observation of the $^{12}C/^{13}C$ isotope effect at C(1) is consistent with the Intramol-DACat mechanism. In addition, the lack of an isotope effect at $C(2)H_3$ of **AP** argues against the involvement of hydrogenation of the **AP** enol.

2.9.3. N–H---O═C Hydrogen Bond. The molecular structure of Λ-*cis*-*α*-Ru$(OCOCH_3)_2$((*R*)-**L**) (**2**) in crystal (Figure 4b) suggests the existence of an sp^3N−H---O═C hydrogen bond. The H---O length is considered to be 2.067−2.112 Å, as judged by the theoretical location of H on N (see top view). In addition, the dihedral angle made by CH_3COO−Ru−N−H is 17.93°. The hydrogen bond, as well as the small dihedral angle, would also be reflected in the **B**/**AP** complex, effecting Intramol-DACat ability to transfer the two hydrogen atoms to the C═O double bond of **AP** via $\mathbf{C}_{Si}$.

2.10. Hydrogenation versus Transfer Hydrogenation. The present asymmetric reduction was proved to proceed via

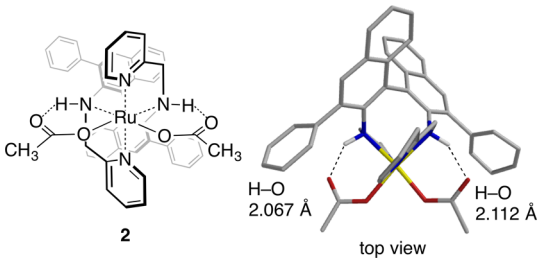

hydrogenation but not via transfer hydrogenation from *i*PrOH as follows.[20,23c,d] Under the standard conditions using $(CH_3)_2CDOH$ instead of *i*PrOH, (*R*)-**PE** and (*S*)-**PE** were quantitatively obtained in a 94:6 ratio. After separation of the enantiomers, the degree of protium incorporation into (*R*)-**PE** and (*S*)-**PE** was determined by ^1H NMR analysis. The relative H signal intensities toward the C_{para}−H signal of the phenyl group ranged from 0.990 to 1.007 (Figure 18). Within the error

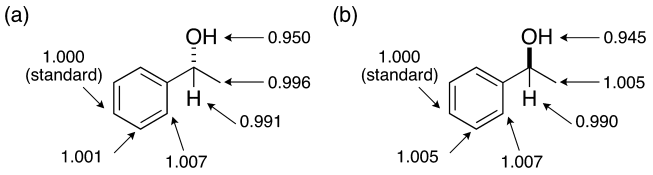

Figure 18. Ratio of protium incorporation in (*R*)-1-phenylethanol ((*R*)-**PE**) (a) and (*S*)-**PE** (b) obtained under the standard conditions using $H_2/(CH_3)_2CDOH$ and H_2/*i*PrOH, respectively (acetone-d_6 with 45° pulse and 30-s relaxation delay).

of the analysis, no **D** was introduced at any carbons of (*R*)-**PE** or (*S*)-**PE**, clearly indicating that a transfer hydrogenation mechanism was not involved in the (*R*)-**L**/**A**-catalyzed reduction. The most likely explanation is that the major and minor products, (*R*)-**PE** and (*S*)-**PE**, are both produced by the same mechanism[17] with an energy difference of 2.07 kcal/mol between $\mathbf{C}_{Re}$ and $\mathbf{C}_{Si}$.

3. CONCLUSION

The present asymmetric hydrogenation of acetophenone (**AP**) using a combined system of (*R*)-Ph-BINAN-H-Py ((*R*)-**L**) and Ru(π-$CH_2C(CH_3)CH_2)_2$(cod) (**A**) proceeds with virtually no change in **L** and **A**, giving (*R*)-**PE** with an *R*/*S* ratio of 97:3.[13] The series of mechanistic studies described has revealed the complete picture of the catalysis, which follows the rate law of $[\mathbf{PE}] = k_0k_2[\mathbf{A}]_0[H_2]^3t^2/2K_{\mathbf{AP}}[\mathbf{AP}]_0$ with $k_0k_2/K_{\mathbf{AP}} = 4.1 \times 10^3$ M^{-2} h^{-2}. The time-squared term relates to two processes occurring in parallel: namely, the preliminary step before the cycle and the cycle itself.

The detailed reaction sequence in the preliminary process is unclear. Most probably, the introductory step would initiate with very slow and irreversible hydrogenolysis of the Ru-π-allyl bonds of **A** with 2-mol amounts of H_2 molecules by generation of $(CH_3)_2C{=}CH_2$,[39] producing a tiny (<1%) amount of an ambiguous RuH_2 species in first-order for $[\mathbf{A}]_0$ and second-order for $[H_2]$. Immediately after its generation, the RuH_2 species is trapped without any energy barrier by the particular tetradentate sp^2N/sp^3NH linear N4 ligand (*R*)-**L**. The characteristics of (*R*)-**L**, including very strong metal capturing ability with a high level of *cis*-*α* selectivity in the formation of octahedral metal complexes, enable the generation of such a delicate Λ-*cis*-*α* **B** intermediate, which works as a very reactive catalyst in the presence of **AP** but readily decomposes in its

DOI: 10.1021/jacs.5b02350
J. Am. Chem. Soc. 2015, 137, 8138−8149

absence. The first- and zeroth-order kinetics observed for $[\mathbf{A}]_0$ and $[\mathbf{L}]_0$, respectively, as well as the minimal effect of $[\mathbf{A}]_0$, $[\mathbf{L}]_0$, and $[H_2]$ (pH_2) on enantioselectivity, excludes the possibility of prior replacement of the cod ligand of **A** with (*R*)-**L**, followed by hydrogenolysis of the Ru-π-allyl bonds. In parallel to its reluctant generation, **B** rapidly converts **AP** to **PE** by means of another H_2 molecule. In the **B** −> **D** step, the NH in **B** quickly captures **AP** to move to a charge-alternating six-membered transition state $\mathbf{C}_{Si}$. Here, the two hydrogen atoms of the polarized $H^{\delta+}-N^{\delta-}$---$Ru^{\delta+}-H^{\delta-}$ moiety are delivered in a concerted manner to the similarly polarized $C^{\delta+}=O^{\delta-}$ of **AP** via the prior formation of an N−H---O═C hydrogen bond, for which the energy barrier is lower than that for the subsequent hydride transfer. The *Si* face of **AP** is selected because of a CH-π attractive interaction between the PyC(6)H of **L** and the aromatic π system of **AP**. The electronic factor surpasses the steric advantage in $\mathbf{C}_{Re}$. The Intramol-DACat mechanism operates in $\mathbf{C}_{Si}$ to give the coordinatively unsaturated Ru amide **D**. This **B** −> **D** step proceeds with a zeroth-order dependence on [**AP**] in the reaction system, but the turnover rate is slowed mainly by the formation of a Ru enolate of **AP**, which is also stabilized by a CH-π attractive interaction. Inhibition from *i*PrOH and (*R*)-**PE** is negligible, but the degree of inhibition by the enantiomeric product (*S*)-**PE** is 15 times higher than that by (*R*)-**PE**.

The reaction frequency of the induction step is $<2.1 \times 10^{-4}$ h^{-1}, while the turnover frequency of the cycle is $>5.7 \times 10^{4}$ h^{-1}.[40] The eight-order difference in these frequencies causes the seemingly unusual phenomenon that **PE** is quantitatively produced without any detectable Ru complex formation. The $\mathbf{L}/\mathbf{A}/2H_2$ to **B** process follows a first-order dependence on $[\mathbf{A}]_0$ and a zeroth-order dependence on $[\mathbf{L}]_0$; as a result, even a 1/100 ratio of **L** (0.02 mM) to **A** (2 mM) maintains high catalytic performance, attaining a chiral multiplication of 87 000.

There are likely to be many other examples in which a negligible amount of reactive and unstable species is operating in catalysis.[41] The present study should stimulate our ideas for the further development of asymmetric molecular catalysis. By using preformed well-defined metal complexes, opportunities to find a high performance catalyst may sometimes be missed.

■ ASSOCIATED CONTENT

Supporting Information

Experimental procedures for NMR study, $^{12}C/^{13}C$ kinetic isotope effect determination, and isotope labeling; experimental and spectroscopic data for the new ligands and Ru complexes; X-ray crystallographic data (CIF); detailed rate law deduction; and kinetic data and graphs. The Supporting Information is available free of charge on the ACS Publications website at DOI: 10.1021/jacs.5b02350.

■ AUTHOR INFORMATION

Corresponding Author

*kitamura@os.rcms.nagoya-u.ac.jp

Notes

The authors declare no competing financial interest.

■ ACKNOWLEDGMENTS

This work was aided by a Grant-in-Aid for Scientific Research (No. 25E07B212 and No. 23005914) from the Ministry of Education, Culture, Sports, Science and Technology (Japan) and an Advanced Catalytic Transformation Program for Carbon Utilization (ACT-C) from Japan Science and Technology Agency (JST). We thank Masahiro Tsuzuki for preliminary kinetic study and Prof. Donna G. Blackmond and Prof. John F. Hartwig for valuable discussions for the kinetics.

■ REFERENCES

(1) (a) Noyori, R.; Ohkuma, T.; Kitamura, M.; Takaya, H.; Sayo, N.; Kumobayashi, H.; Akutagawa, S. *J. Am. Chem. Soc.* **1987**, *109*, 5856−5858. (b) Kitamura, M.; Ohkuma, T.; Inoue, S.; Sayo, N.; Kumobayashi, H.; Akutagawa, S.; Ohta, T.; Takaya, H.; Noyori, R. *J. Am. Chem. Soc.* **1988**, *110*, 629−631. See also: (c) Kitamura, M.; Nakatsuka, H. *Chem. Commun.* **2011**, *47*, 842−846. (d) Noyori, R.; Kitamura, M.; Ohkuma, T. *Proc. Natl. Acad. Sci. U.S.A.* **2004**, *101*, 5356−5362.

(2) (a) Calvin, M. *Trans. Faraday Soc.* **1938**, *34*, 1181−1191. (b) Calvin, M. *J. Am. Chem. Soc.* **1939**, *61*, 2230−2234.

(3) (a) James, B. R. *Homogeneous Hydrogenation*; Wiley: New York, 1974; pp 1−525. (b) Birch, A. J.; Williamson, D. H. *Org. React.* **1976**, *24*, 1−186. (c) James, B. R. Addition of Hydrogen and Hydrogen Cyanide to Carbon−Carbon Double and Triple Bonds. In *Comprehensive Organometallic Chemistry*; Wilkinson, G., Stone, F. G. A., Abel, E. W., Eds.; Pergamon Press: Oxford, U.K., 1982; Vol. *8*, pp 285−369. For a recent review, see: (d) Tsukamoto, M.; Kitamura, M. Reduction by Homogeneous Catalysis or Biocatalysis. In *Science of Synthesis, Houben−Weyl Methods of Molecular Transformations*; Hiemstra, H., Schaumann, E., Eds.; Thieme: Stuttgart, Germany, 2009; Vol. *48*, Chapter 48.1.3.6.2, pp 341−357.

(4) Schrock, R. R.; Osborn, J. A. *Chem. Commun.* **1970**, 567−568.

(5) (a) Bonvicini, P.; Levi, A.; Modena, G.; Scorrano, G. *J. Chem. Soc., Chem. Commun.* **1972**, 1188−1189. (b) Tanaka, M.; Watanabe, Y.; Mitsudo, T.; Iwane, H.; Takegami, Y. *Chem. Lett.* **1973**, *2*, 239−240. (c) Sih, C. J.; Heather, J. B.; Peruzzotti, G. P.; Price, P.; Sood, R.; Lee, L.-F. H. *J. Am. Chem. Soc.* **1973**, *95*, 1676−1677. (d) Solodar, J. *Chem. Technol.* **1975**, 421−423. (e) Levi, A.; Modena, G.; Scorrano, G. *J. Chem. Soc., Chem. Commun.* **1975**, 6−7. (f) Heil, B.; Törös, S.; Vastag, S.; Markó, L. *J. Organomet. Chem.* **1975**, *94*, C47−C48. (g) Hayashi, T.; Mise, T.; Kumada, M. *Tetrahedron Lett.* **1976**, *17*, 4351−4354. (h) Fiorini, M.; Marcati, F.; Giongo, G. M. *J. Mol. Catal.* **1977/1978**, *3*, 385−387. (i) Ojima, I.; Kogure, T.; Achiwa, K. *J. Chem. Soc., Chem. Commun.* **1977**, 428−430. (j) Törös, S.; Heil, B.; Kollár, L.; Markó, L. *J. Organomet. Chem.* **1980**, *197*, 85−86.

(6) Reviews and books: (a) Noyori, R.; Kitamura, M. Enantioselective Catalysis with Metal Complexes. An Overview. In *Modern Synthetic Methods*; Scheffold, R., Ed.; Springer Verlag: Berlin/Heidelberg, Germany, 1989; pp 115−198. (b) Noyori, R. *Angew. Chem., Int. Ed.* **2002**, *41*, 2008−2022. (c) Kitamura, M.; Noyori, R. Hydrogenation and Transfer Hydrogenation. In *Ruthenium in Organic Synthesis*; Murahashi, S.-I., Ed.; Wiley-VCH: Weinheim, Germany, 2004; pp 3−52. (d) Ohkuma, T.; Kitamura, M.; Noyori, R. Ligand Design for Catalytic Asymmetric Reduction. In *New Frontiers in Asymmetric Catalysis*; Mikami, K., Lautens, M., Eds.; John Wiley & Sons: Weinheim, Germany, 2007; pp 1−32.

(7) For the original reaction establishing DACat, see: (a) Kitamura, M.; Suga, S.; Kawai, K.; Noyori, R. *J. Am. Chem. Soc.* **1986**, *108*, 6071−6072. (b) Noyori, R.; Kitamura, M. *Angew. Chem., Int. Ed. Engl.* **1991**, *30*, 49−69. Redox-mediated DACat: (c) Kitamura, M.; Miyata, K.; Seki, T.; Vatmurge, N.; Tanaka, S. *Pure Appl. Chem.* **2013**, *85*, 1121−1132.

(8) Kitamura, M.; Tokunaga, M.; Noyori, R. *J. Org. Chem.* **1992**, *57*, 4053−4054.

(9) (a) Ohkuma, T.; Ooka, H.; Hashiguchi, S.; Ikariya, T.; Noyori, R. *J. Am. Chem. Soc.* **1995**, *117*, 2675−2676. (b) Noyori, R.; Ohkuma, T. *Angew. Chem., Int. Ed.* **2001**, *40*, 40−73. For the asymmetric hydrogenation of *tert*-alkyl ketones, see: (c) Ohkuma, T.; Sandoval, C. A.; Srinivasan, R.; Lin, Q.; Wei, Y.; Muñiz, K.; Noyori, R. *J. Am. Chem. Soc.* **2005**, *127*, 8288−8289.

(10) (a) Shang, G.; Li, W.; Zhang, X. Transition Metal-Catalyzed Homogeneous Asymmetric Hydrogenation. In *Catalytic Asymmetric*

DOI: 10.1021/jacs.5b02350
J. Am. Chem. Soc. 2015, 137, 8138−8149

Synthesis, 3rd ed.; Ojima, I., Ed.; John Wiley & Sons, Inc.: Hoboken, NJ, 2010; pp 343−436. (b) Tang, W.; Zhang, X. *Chem. Rev.* **2003**, *103*, 3029−3069.
(11) Yoon, T. P.; Jacobsen, E. N. *Science* **2003**, *299*, 1691−1693.
(12) Ohgo, Y.; Takeuchi, S.; Yoshimura, J. *Bull. Chem. Soc. Jpn.* **1971**, *44*, 583.
(13) Huang, H.; Okuno, T.; Tsuda, K.; Yoshimura, M.; Kitamura, M. *J. Am. Chem. Soc.* **2006**, *128*, 8716−8717.
(14) H-BINAN-H-Py: Goodwin, H. A.; Lions, F. *J. Am. Chem. Soc.* **1960**, *82*, 5013−5023.
(15) Diamine−Ru, −Rh, −Ir, or −Pd: (a) Pinel, C.; Gendreau-Diaz, N.; Bréhéret, A.; Lemaire, M. *J. Mol. Catal. A: Chem.* **1996**, *112*, L157−L161. (b) Ito, M.; Hirakawa, M.; Murata, K.; Ikariya, T. *Organometallics* **2001**, *20*, 379−381. (c) Hedberg, C.; Källström, K.; Arvidsson, P. I.; Brandt, P.; Andersson, P. G. *J. Am. Chem. Soc.* **2005**, *127*, 15083−15090. (d) Utsumi, N.; Tsutsumi, K.; Watanabe, M.; Murata, K.; Arai, N.; Kurono, N.; Ohkuma, T. *Heterocycles* **2010**, *80*, 141−147. Shiff base−Ru: (e) Karamé, I.; Jahjah, M.; Messaoudi, A.; Tommasino, M. L.; Lemaire, M. *Tetrahedron: Asymmetry* **2004**, *15*, 1569−1581. Thiourea−Ru: (f) Tommasino, M. L.; Casalta, M.; Breuzard, J. A. J.; Lemaire, M. *Tetrahedron: Asymmetry* **2000**, *11*, 4835−4841. For the importance of N4 ligands, see: (g) He, Y.-M.; Fan, Q.-H. *Org. Biomol. Chem.* **2010**, *8*, 2497−2504. (h) Yoshimura, M.; Tanaka, S.; Kitamura, M. *Tetrahedron Lett.* **2014**, *55*, 3635−3640.
(16) Powell, J.; Shaw, B. L. *J. Chem. Soc. A* **1968**, 159−161.
(17) Ishibashi, Y.; Bessho, Y.; Yoshimura, M.; Tsukamoto, M.; Kitamura, M. *Angew. Chem., Int. Ed.* **2005**, *44*, 7287−7290.
(18) (a) Stebler-Röthlisberger, M.; Ludi, A. *Polyhedron* **1986**, *5*, 1217−1221. (b) Luginbühl, W.; Zbinden, P.; Pittet, P. A.; Armbruster, T.; Bürgi, H.-B.; Merbach, A. E.; Ludi, A. *Inorg. Chem.* **1991**, *30*, 2350−2355.
(19) Lindsay, A. J.; Wilkinson, G.; Motevalli, M.; Hursthouse, M. B. *J. Chem. Soc., Dalton Trans.* **1985**, 2321−2326.
(20) For details, see Supporting Information.
(21) (a) Abdur-Rashid, K.; Faatz, M.; Lough, A. J.; Morris, R. H. *J. Am. Chem. Soc.* **2001**, *123*, 7473−7474. (b) Abdur-Rashid, K.; Clapham, S. E.; Hadzovic, A.; Harvey, J. N.; Lough, A. J.; Morris, R. H. *J. Am. Chem. Soc.* **2002**, *124*, 15104−15118. (c) Clapham, S. E.; Hadzovic, A.; Morris, R. H. *Coord. Chem. Rev.* **2004**, *248*, 2201−2237. (d) Abbel, R.; Abdur-Rashid, K.; Faatz, M.; Hadzovic, A.; Lough, A. J.; Morris, R. H. *J. Am. Chem. Soc.* **2005**, *127*, 1870−1882. (e) Hadzovic, A.; Song, D.; MacLaughlin, C. M.; Morris, R. H. *Organometallics* **2007**, *26*, 5987−5999. (f) O, W. W. N.; Lough, A. J.; Morris, R. H. *Organometallics* **2011**, *30*, 1236−1252.
(22) (a) Daley, C. J. A.; Bergens, S. H. *J. Am. Chem. Soc.* **2002**, *124*, 3680−3691. (b) Hamilton, R. J.; Leong, C. G.; Bigam, G.; Miskolzie, M.; Bergens, S. H. *J. Am. Chem. Soc.* **2005**, *127*, 4152−4153. (c) Hamilton, R. J.; Bergens, S. H. *J. Am. Chem. Soc.* **2006**, *128*, 13700−13701. (d) Hamilton, R. J.; Bergens, S. H. *J. Am. Chem. Soc.* **2008**, *130*, 11979−11987. (e) Takebayashi, S.; Bergens, S. H. *Organometallics* **2009**, *28*, 2349−2351.
(23) (a) Yamakawa, M.; Yamada, I.; Noyori, R. *Angew. Chem., Int. Ed.* **2001**, *40*, 2818−2821. (b) Sandoval, C. A.; Ohkuma, T.; Muñiz, K.; Noyori, R. *J. Am. Chem. Soc.* **2003**, *125*, 13490−13503. (c) Sandoval, C. A.; Ohkuma, T.; Utsumi, N.; Tsutsumi, K.; Murata, K.; Noyori, R. *Chem.—Asian J.* **2006**, *1*, 102−110. (d) Ohkuma, T.; Utsumi, N.; Tsutsumi, K.; Murata, K.; Sandoval, C. A.; Noyori, R. *J. Am. Chem. Soc.* **2006**, *128*, 8724−8725.
(24) (a) Zhang, J.; Leitus, G.; Ben-David, Y.; Milstein, D. *J. Am. Chem. Soc.* **2005**, *127*, 10840−10841. (b) Zhang, J.; Leitus, G.; Ben-David, Y.; Milstein, D. *Angew. Chem., Int. Ed.* **2006**, *45*, 1113−1115.
(25) Prechtl, M. H. G.; Ben-David, Y.; Giunta, D.; Busch, S.; Taniguchi, Y.; Wisniewski, W.; Görls, H.; Mynott, R. J.; Theyssen, N.; Milstein, D.; Leitner, W. *Chem.—Eur. J.* **2007**, *13*, 1539−1546.
(26) Goliaszewski, A.; Schwartz, J. *Tetrahedron* **1985**, *41*, 5779−5789.
(27) (a) vom Stein, T.; Weigand, T.; Merkens, C.; Klankermayer, J.; Leitner, W. *ChemCatChem* **2013**, *5*, 439−441. (b) vom Stein, T.; Meuresch, M.; Limper, D.; Schmitz, M.; Hölscher, M.; Coetzee, J.; Cole-Hamilton, D. J.; Klankermayer, J.; Leitner, W. *J. Am. Chem. Soc.* **2014**, *136*, 13217−13225.
(28) (a) Bau, R.; Teller, R. G.; Kirtley, S. W.; Koetzle, T. F. *Acc. Chem. Res.* **1979**, *12*, 176−183. (b) Venanzi, L. M. *Coord. Chem. Rev.* **1982**, *43*, 251−274.
(29) (a) Six, C.; Gabor, B.; Görls, H.; Mynott, R.; Philipps, P.; Leitner, W. *Organometallics* **1999**, *18*, 3316−3326. (b) Schweda, L.; Nader, A.; Menzel, R.; Biletzki, T.; Johne, C.; Görls, H.; Imhof, W. *J. Organomet. Chem.* **2010**, *695*, 2076−2082.
(30) Chiang, Y.; Kresge, A. J.; Santaballa, J. A.; Wirz, J. *J. Am. Chem. Soc.* **1988**, *110*, 5506−5510.
(31) Mehta, S. P. S.; Mehrotra, R. N. *Transition Met. Chem.* **1991**, *16*, 402−406.
(32) Wade, L. G. *Organic Chemistry*; Prentice Hall: Upper Saddle River, NJ, 1999.
(33) For Ru *O*-enolates and Rh *O*-enolates, see: ref 21b. (a) Hartwig, J. F.; Bergman, R. G.; Andersen, R. A. *J. Am. Chem. Soc.* **1990**, *112*, 3234−3236. (b) Slough, G. A.; Bergman, R. G.; Heathcock, C. H. *J. Am. Chem. Soc.* **1989**, *111*, 938−949. Regarding the possibility that the Ru *C*-enolate is the inhibitory factor, see: ref 23c.
(34) There may be an NH-π stabilization. For the related report, see: Sandoval, C. A.; Shi, Q.; Liu, S.; Noyori, R. *Chem.—Asian J.* **2009**, *4*, 1221−1224.
(35) Soai, K.; Shibata, T.; Morioka, H.; Choji, K. *Nature* **1995**, *378*, 767−768.
(36) The concentration of hydrogen was estimated to be 0.18 M at 50 atm of pH_2; see Brunner, E. *Ber. Bunsenges. Phys. Chem.* **1979**, *83*, 715−721.
(37) Clockwise and anticlockwise mode is changed when the oxygen lone pair cis to aryl group is selected.
(38) Singleton, A. D.; Thomas, A. A. *J. Am. Chem. Soc.* **1995**, *117*, 9357−9358.
(39) Detection of $(CH_3)_2C{=}CH_2$ and cod was difficult because, at most, **B** was generated only 10/177 mM under the ^{1}H NMR monitoring conditions (Figure 6).
(40) The k_0 value was assumed to be 6.46×10^{-3} M^{-2} h^{-1} at most, as estimated from the S/N ratio of 177 observed in the ^{1}H NMR analysis (Figure 6b). By use of the values of k_0, $[H_2] = 0.18$ M, $[\mathbf{AP}]_0 = 2$ M, and $k_0k_2/K_{\mathbf{AP}} = 4.1 \times 10^3$ M^{-2} h^{-2}, the frequency of the generation of **B** from **A** ($v_0/[\mathbf{A}]_0 = k_0[H_2]^2$) and the turnover frequency of **B**-catalyzed hydrogenation ($v_2/[Ru_{cycle}] = k_2[H_2]/K_{\mathbf{AP}}[\mathbf{AP}]_0 = (k_0k_2/K_{\mathbf{AP}})(1/k_0)([H_2]/[\mathbf{AP}]_0)$) are calculated to be $<2.1 \times 10^{-4}$ and $>5.7 \times 10^4$ h^{-1}, respectively. Here, v_0 is defined as $-d[\mathbf{A}]/dt = k_0[\mathbf{A}]_0[H_2]^2$, and v_2 is defined as $d[\mathbf{PE}]/dt = k_2[Ru_{cycle}][H_2]/K_{\mathbf{AP}}[\mathbf{AP}]_0$.
(41) For some examples, see: (a) Brunel, J. M.; Heumann, A.; Buono, G. *Angew. Chem., Int. Ed.* **2000**, *39*, 1946−1949. (b) Makio, H.; Kashiwa, N.; Fujita, T. *Adv. Synth. Catal.* **2002**, *344*, 477−493.

DOI: 10.1021/jacs.5b02350
J. Am. Chem. Soc. 2015, 137, 8138−8149